Table 1. Comparison of Baseline Clinical Characteristics

	HIP (n=116)	Non-HIP (n=101)	p Values
Age (yrs)	69 ± 8	68 ± 9	0.39
Male gender	99 (85%)	89(82%)	0.41
Diabetes mellitus	35 (30%)	32 (32%)	0.81
Hypertension	79 (68%)	61(60%)	0.24
Smoking	30 (26%)	30 (30%)	0.52
BMI (kg/m^2)	24.2 ± 2.5	23.8 ± 3.7	0.35
Total cholesterol (mg/dL)	198 ± 37	199 ± 40	0.84
HDL cholesterol (mg/dL)	43 ± 11	48 ± 16	0.007
LDL cholesterol (mg/dL)	136 ± 31	125 ± 29	0.008
hs-CRP (mg/dL)*	2.1 (1.0, 3.6)	1.35 (0.5, 2.3)	0.001
IMT (mm)	2.47 ± 1.0	1.67 ± 1.0	<0.001
Carotid artery stenosis (%)*	22.5 (15.0, 46.1)	20.5 (9.0, 4.9)	0.97
Medications			
Aspirin	110 (95%)	98 (97%)	0.41
Beta-blocker	67(58%)	62 (61%)	0.59
Statin	71 (61%)	64 (63%)	0.74
ACEI or ARB	50 (43%)	47 (47%)	0.61
Multi-vessel CAD	55 (55%)	31 (31%)	0.01
LV dysfunction (EF < 40%) (%)	8 (7%)	6 (6%)	0.77
Previous MI	42 (36%)	21 (21%)	0.01

Data are presented as the mean ± SD or number (%) of patients. *Median, first quartile, and third quartile. ACE = angiotensin-converting enzyme inhibitor; ARB = angiotensin II receptor blocker; BMI = body mass index; CAD; coronary artery disease; hs-CRP = high sensitivity C-reactive protein; HIP = high-intensity plaques; EF = ejection fraction; HDL; high-density lipoprotein; IMT = maximum intima-media thickness; LDL = low-density lipoprotein; LV = left ventricular; MI = myocardial infarction.

Table 2. Summary of coronary events during the follow-up period in patients with coronary artery disease

	HIP (n=116)	Non-HIP (n=101)	p Values
Composite end-points	31	5	< 0.001
Cardiac death	4	0	0.125
Non-fatal acute MI	4	1	0.375
Unstable angina	16	2	0.002
Hospitalization for recurrent angina	7	2	0.180

Abbreviations as in Table 1.

Table 3. Univariate analysis of risk factors for a coronary event in patients with coronary artery disease

	Hazard ratio	95% CI	p Values
Age (yrs)	1.02	0.98–1.05	0.60
Male gender	1.71	0.72–3.32	0.29
Diabetes mellitus	1.68	0.88–4.41	0.15
Hypertension	0.89	0.47–1.61	0.71
Smoking	1.51	0.68–2.99	0.28
BMI (kg/m^2)	0.98	0.79–1.01	0.18
Total cholesterol (mg/dL)	0.86	0.71–1.00	0.17
HDL cholesterol (mg/dL)	0.95	0.98–1.05	0.21
LDL cholesterol (mg/dL)	1.12	0.98–1.05	0.35
hs-CRP (mg/dL)	1.41	1.02–1.51	0.03
IMT(mm)	1.55	1.12–1.89	0.004
Multi-vessel CAD	2.18	1.21–6.12	0.001
LV dysfunction (EF < 40%)	1.70	0.81–2.33	0.11
Previous MI	1.95	1.19–5.35	0.001
Presence of HIP	1.76	1.21–3.32	<0.001

CI = confidence interval; other abbreviations as in Table 1.

Table 4. Multivariate Cox regression analysis of risk factors for a coronary event

	β	SE	Hazard Ratio	p Value	95% CI
Presence of HIP	1.130	0.291	3.10	< 0.0001	1.79–5.01
IMT (mm) (> 2.78 mm)	0.581	0.201	1.79	0.021	1.19–4.01
hs-CRP (> 3.0 mg/dL)	0.334	0.179	1.40	0.099	0.94–2.02
Previous MI	0.168	0.20	1.18	0.401	0.56–1.22
Multi-vessel CAD	0.268	0.206	1.31	0.194	0.51–1.15

Abbreviations as in Table 1.

Journal of Nuclear Medicine, published on April 15, 2011 as doi:10.2967/jnumed.110.084848

Experimental Pig Model of Old Myocardial Infarction with Long Survival Leading to Chronic Left Ventricular Dysfunction and Remodeling as Evaluated by PET

Noboru Teramoto[1], Kazuhiro Koshino[1], Ikuo Yokoyama[2,3], Shigeru Miyagawa[4], Tsutomu Zeniya[1], Yoshiyuki Hirano[1], Hajime Fukuda[1], Junichiro Enmi[1], Yoshiki Sawa[4], Juhani Knuuti[5], and Hidehiro Iida[1]

[1]Department of Investigative Radiology, National Cerebral and Cardiovascular Center Research Institute, Osaka, Japan; [2]School of Medicine and Faculty of Medicine, The University of Tokyo, Tokyo, Japan; [3]Department of Cardiovascular Medicine, Sanno Hospital, International University of Health and Welfare, Tokyo, Japan; [4]Department of Cardiac Surgery, Osaka University, School of Medicine, Osaka, Japan; and [5]Turku PET Centre, University of Turku, Turku, Finland

A pig model of reduced left ventricular (LV) function and remodeling or chronic heart failure with long survival after myocardial infarction (MI) has not been established. The aim of this study was to evaluate the pathophysiologic status of a pig model of old MI using a series of PET studies. **Methods:** Twenty-seven male farm pigs were divided into 2 groups: 7 animals in the control group and 20 animals that underwent a proximal coronary artery (CA) occlusion using an ameroid constrictor after distal CA ligation. A series of PET examinations was performed to assess LV volumes, LV functions, myocardial perfusion response to adenosine, and viability as water-perfusable tissue index. **Results:** The distal CA ligation inhibited arrhythmia during and after the operation, and a transmural anteroseptal MI, with an infarction area of 27% ± 5% of the whole left ventricle, was generated with a survival rate of 75% at 4 mo. Wall motion evaluated by ^{18}F-FDG PET was diffusely reduced, including the noninfarcted wall. Global LV ejection fraction as assessed by gated $C^{15}O$ PET was reduced (39% ± 16%) in the group undergoing occlusion, compared with the control group (66% ± 16%, $P < 0.05$). LV end-systolic (31.4 ± 9.2 cm^3) and end-diastolic (52.7 ± 10.2 cm^3) volumes were increased, compared with controls (15.2 ± 9.4 cm^3, $P < 0.01$, and 41.7 ± 11.5 cm^3, $P < 0.05$, respectively). Histology showed hypertrophy and development of microscopic fibrosis in noninfarcted myocardium. PET demonstrated the reduced myocardial perfusion response to adenosine and also reduced water-perfusable tissue index in remote segments. **Conclusion:** The pig model of old MI generated by the chronic proximal CA obstruction after distal ligation was characterized by LV dysfunction and remodeling, with a high survival rate.

Key Words: experimental model; PET; myocardial flow reserve; remodeling; regeneration therapy

J Nucl Med 2011; 52:761–768
DOI: 10.2967/jnumed.110.084848

Chronic heart failure (CHF) is an increasing health concern (*1*). Myocardial infarction (MI) is the cause of CHF in two thirds of the patients, and the morbidity and mortality remain high (*2,3*). The potential therapies, such as new class of pharmacologic agents and cell therapy (*4*), need to be tested in proper animal models to demonstrate the effects and outcome before initiating clinical trials. Dogs have been extensively used in heart research. Because the coronary arterial systems in dogs can develop collaterals quickly when myocardial ischemia occurs, it has been difficult to produce a large MI that typically introduces CHF with general characteristics of left ventricular (LV) remodeling (*5*).

Pigs have been considered better suited than dogs for pathophysiologic research of ischemic heart diseases, because the coronary system of pigs is more similar to that of humans (*6*). Tolerance of ischemia and denervation after ischemia in pigs is also similar to that in humans (*6*). Because of the delayed development of collaterals after occlusion, ligation of a peripheral part of the coronary arterial system generates a small MI (*7*). However, an experimental model of large MI introducing global LV dysfunction is difficult to develop, because sudden cardiac death (SCD) due to fatal arrhythmias and an intolerance of ischemia frequently occurs in pigs (*8*). The models of small MI made by the ligation of a peripheral part of the coronary arterial system demonstrate reasonably good survival rates but only for a small infarction. The model of small MI using a coronary ameroid constrictor (model MRI-2.50-TI; Research Instruments SW) has also demonstrated moderate SCD rates (*6,8–13–15*), but the animals develop primarily chronic ischemia or hibernating myocardium, without a significant amount of scar tissue. Thus, the limitations of current models are that the infarcted region is small and that the hearts are not developing a clinical picture of CHF with global LV dysfunction, LV dilatation, and remodeling.

On the other hand, Shen et al. (*16*) developed an experimental pig model of MI and heart failure. Sequential

Received Oct. 30, 2010; revision accepted Dec. 9, 2010.
For correspondence or reprints contact: Hidehiro Iida, Department of Investigative Radiology, National Cardiovascular Center Research Institute, 5-7-1 Fujishiro-dai, Suita City, Osaka, Japan 565-8565.
E-mail: iida@ri.ncvc.go.jp

ligation of distal and proximal coronary arteries was used to establish MI with a reasonable survival rate, and pacing tachycardia was used to achieve heart failure. However, this pig model was studied over only a short term (21 d) and required pacing tachycardia to cause CHF. There has been little evaluation of pathophysiology and no evidence of the presence of cardiac remodeling.

This aim of this study was to characterize the pig model of old MI. We first reinvestigated the technique of generating a pig model of relatively large MI causing global LV dysfunction and LV remodeling in segments remote from the infarcted region, by means of the sequential ligation of distal and proximal coronary arteries without the pacing procedures. We then evaluated the pathophysiologic characteristics of this animal model by comprehensively analyzing histology, LV volumes and LV function, myocardial perfusion response to adenosine, and perfusable tissue fractions (PTF) in the remote segment, using an advanced PET technique.

MATERIALS AND METHODS

Subjects

Male farm pigs, 3 mo old at the start of the study (weight range, 18–23 kg; mean weight ± SD, 20 ± 1.2 kg), were used. The animals were divided into 2 groups. Group A consisted of 7 pigs without any operation and was designated as the control group (average body weight, 26 ± 2.4 kg). Group B consisted of 20 pigs that underwent occlusion using an ameroid constrictor (*7*); ligation of the distal left anterior descending coronary artery (LAD) was performed before the ameroid constrictor was used. Of the 16 pigs that survived for 4 mo after the operation, 7 underwent PET studies. The other 9 were assigned to tissue-regenerative projects. The average body weight of this group of 7 pigs was 42 ± 8.2 kg at the time of the PET scan.

Animals were maintained and handled in accordance with guidelines for animal research (*17*). The study protocol was approved by the local Committee for Laboratory Animal Welfare, National Cardiovascular Center, Osaka, Japan.

Permanent Occlusion Procedures

In group B, permanent occlusion was made at the proximal LAD using an ameroid constrictor (*18*) (Fig. 1) as follows. Pigs were preanesthetized by an intramuscular injection of ketamine hydrochloride (20 mg/kg; Ketaral [Diichi-Sankyo]) and xylazine hydrochloride (2 mg/kg; Celactal [Bayer HealthCare]). The animals were positioned supine, and a 22-gauge indwelling needle (Surflo F&F; Terumo) was inserted in the central vein of the auricle. A 3-way cock (Terufusion TS-TR2K; Terumo) was attached to the external cylinder of the indwelling needle and connected for continuous anesthetic injection. The animals were intubated with an endotracheal cannula (6 French; Sheridan) and then connected to an artificial respirator (Single Animal Volume Controlled Ventilators model 613 [Harvard Apparatus]) with a stroke volume of 200–300 cm^3/stroke and frequency of 20/min. Propofol (6 mg/kg/h; Diprivan [Astra-Zeneca]) and vecuronium bromide (0.05 mg/kg/h; Musculux [Sankyo Yell Yakuhin Co., Ltd.]) were continuously infused using a syringe pump (Terufusion TE-3310N; Terumo). Then, the animals were fixed in a recumbent position so that the left thorax was exposed, and the outer layer of skin and muscles between the third and fourth ribs was dissected. The distance between the third and fourth ribs was widened with a rib spreader to allow a direct view of the left auricle and LAD. The pericardium was dissected along the LAD, from the upper part of the left auricle (~6 cm), to expose the myocardium around the LAD. The LAD on the proximal side, below the left auricle from the myocardium, was exfoliated for approximately 1 cm. A lidocaine hydrochloride jelly (Xylocaine jelly; Astra-Zeneca) was applied to anesthetize the area.

A complete ligation was first made on the distal LAD (no. 9), immediately after the second diagonal branch, using a suture (2-0; Nescosuture) approximately 20 min before the ameroid constrictor was fastened. An ameroid constrictor (COR-2.50-SS; Research Instruments) was then fastened using sutures as displayed in Figure 1. To enhance the effect of the ameroid constrictor, 2 additional suture strings were loosely rounded at the site of the ameroid so that these strings were located between (below) the ameroid constrictor and arterial wall.

PET Procedures

After fasting overnight, the pigs were sedated with ketamine hydrochloride (20 mg/kg) and xylazine hydrochloride (2 mg/kg) by intramuscular injection. Anesthesia was induced and maintained with intravenous propofol (6 mg/kg/h) and vecuronium bromide (0.05 mg/kg/h). The animals were intubated and mechanically ventilated with a mixture of 25% oxygen and 75% nitrogen at 10 mL/kg plus 50 mL/stroke at 20 strokes/min. Catheters were placed in the femoral artery to monitor the arterial blood pressure and in the femoral vein to infuse $H_2{}^{15}O$ or ^{18}F-labeled FDG. Systolic and diastolic blood pressure, heart rate, and arterial blood gases were monitored.

A series of PET scans was obtained using an ECAT-HR tomograph (CTI Inc.). The blood-pool images were obtained after the animals inhaled 2.7 GBq of $C^{15}O$ gas (*19*). Arterial blood samples were taken every minute during the $C^{15}O$ scan, and their radioactivity concentration in the whole blood was measured. Additional electrocardiogram-gated $C^{15}O$ images were obtained (16 gates). After 12–15 min of ^{15}O radioactivity decay, 7 dynamic $H_2{}^{15}O$ PET scans were acquired at intervals of 12–15 min. The first and the last scans were obtained without pharmacologic stress, and the second through sixth scans were obtained during intravenous infusion of adenosine (100, 200, 400, 600, and 800

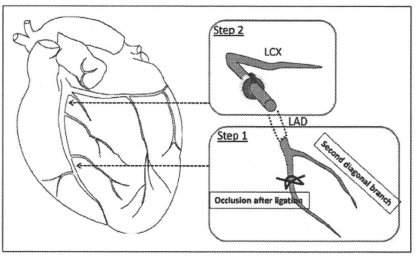

FIGURE 1. Ligation of LV LAD. Distal LAD after second diagonal branch was ligated, and 30 min later ameroid constrictor was placed at proximal LAD. Two suture strings were inserted between ameroid constrictor and arterial wall to make occlusion complete. LCX = left circumflex artery.

jnm084848-pm ■ 4/15/11

[only for group A] μg/kg/min). The 6-min dynamic scan of 26 frames (12 × 5, 8 × 15, and 6 × 30 s) was started when radioactivity appeared in the right ventricle. Furthermore, another PET scan using ^{18}F-FDG was acquired using a euglycemic hyperinsulinemic clamp (*20,21*). For this study, insulin (4 mIU/kg/h) and glucose (5–8 mg/kg/min) were continuously infused over 2 h, and then approximately 111 MBq of ^{18}F-FDG was intravenously injected. The blood glucose was 109 ± 10.6, 105 ± 3.8, and 107 ± 10.0 mg/dL at the time of ^{18}F-FDG injection. PET images were acquired dynamically for 60 min, and the images acquired during the last 30 min were used for further analysis. An additional electrocardiogram-gated scan was obtained for 30 min to estimate myocardial wall motion and wall thickening.

After the PET scans, coronary angiography was undertaken to confirm the occlusion of LAD. A portable angiographic camera (Digital Mobile Imaging System OEC Series 9800; GE Healthcare U.K. Ltd.) was used with the contrast medium (Omnipaque 300; Daiichi-Sankyo).

Histologic Analysis

At the end of the study, pentobarbital sodium was administered, and animals were euthanized. The animals' hearts were then excised and sliced at a thickness of 10 mm to correspond to PET images (*22*). The slices were stained with Masson trichrome and hematoxylin and eosin. The surface area of the infarcted LV wall on the stained slices was calculated according to a previously describe procedure (*22*). The length of the infarcted zone, including both transmural and nontransmural infarction, was measured on each of the stained slices along the LV wall. The defect surface area was then calculated as a summation of the defect length multiplied by the slice interval. The cell and microvascular structures were also analyzed. In particular, development of fibrosis, cell enlargement, and degeneration of the vascular network were visually estimated. The analysis was masked from the other analyses.

Data Analysis

The extravascular tissue density images (g/mL) were calculated by subtracting the C^{15}O blood volume from the transmission images (*23*). The relative images of myocardial blood flow (MBF) and water-PTF (g/mL) were also generated from the dynamic $H_2{}^{15}O$ images (*22,23*). The relative accumulation of ^{18}F-FDG was calculated using validated techniques (*24*). The regions of interest were placed in the anterior wall and lateral–anterior wall, which corresponded to the MI and normal-tissue regions, respectively. The regions of interest were then copied to other images, and the quantitative parameters of regional MBF (mL/min/g), PTF (g/mL), and arterial blood volume V_a (mL/mL) were calculated using nonlinear least-squares fitting as described previously (*22,23*). These calculations were done for all $H_2{}^{15}O$ PET studies to estimate baseline MBF and the adenosine-based responses both in MI and in non-MI regions.

The water-perfusable tissue index (PTI) (*23,25,26*), which was defined as the fraction of water-perfusable tissue over total tissue, was calculated by dividing PTF by the extravascular tissue density images. This calculation was done for each myocardial region and compared between the infarcted anterior wall and normal posterior–lateral wall regions. The obtained values were also compared with control subjects.

The LV ejection fraction and cardiac output were evaluated by counting the total counts within the LV area from the typical electrocardiogram-gated C^{15}O images shown in Figure 2. The wall motion was analyzed using electrocardiogram-gated ^{18}F-FDG images. The wall motion score was divided into 4 levels (normal, 0; hypokinetic, 1; akinetic, 2; and dyskinetic, 3) and defined for the anterior wall and contralateral (lateral–posterior) wall regions. [Fig. 2]

The surface area of the infarcted LV wall on the ^{18}F-FDG and PTF images was calculated as described previously (*22*). A significant defect was defined as a value less than 50% of that in the control region, which was defined in the contralateral region, indicating preserved ^{18}F-FDG, preserved PTF, and elevated MBF during adenosine. The myocardial midlines were then traced along the 50% of peak count boundary of the C^{15}O blood volume images at each slice (*22*). The surface area of the defect was calculated as a summation of the defect length multiplied by the slice interval. These defect surface areas were compared with those obtained from the stained slices.

All data were presented as mean ± SD. Pearson correlation and linear regression analyses were used to evaluate relationships between the 2 values. A P value of less than 0.05 was considered statistically significant.

RESULTS

Survival Rates of Animal Groups

No adverse events were detected in group A; in group B, 4 pigs (20%) died within a month and an additional pig 1 mo after that. Thus, the total survival rate at 4 mo was 75% in group B. Severe arrhythmia occurred in all animals in group B during the operation. The arrhythmia and fibrillation, introducing the sudden cardiac death, were significantly suppressed at approximately 20 min after ligation of the distal LAD. Figure 3 displays the survival rates of the pigs that underwent the operation. [Fig. 3]

Of the pigs in group B that survived for 4 mo, 7 were selected for further characterization and imaging studies. These 7 animals were compared against the animals in group A, on which no operation was performed. The characteristics of the 2 groups at the time of the imaging

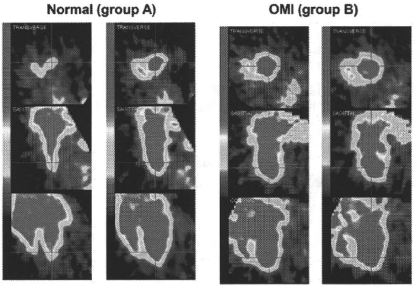

RGB

FIGURE 2. Typical images obtained from electrocardiogram-gated PET scans with C^{15}O inhalation at end-systolic and end-diastolic phases. OMI = old MI.

23
jnm084848-pm ■ 4/15/11

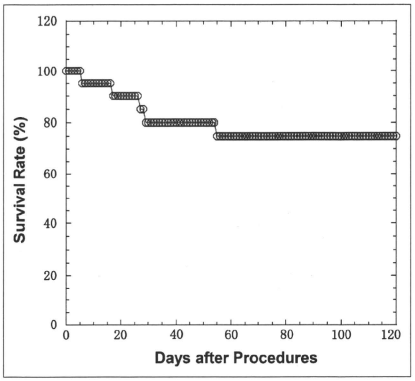

FIGURE 3. Survival rates for group B after ameroid constrictor was placed.

[Table 1] studies are displayed in Table 1. Because the animals in group B were allowed to grow after operation, they were larger at the time of the imaging studies.

Characteristics of Groups

Table 1 shows the hemodynamic data for the animals in groups A and B. Compared with group A, group B showed a significantly reduced heart rate and diastolic blood pressure and, thus, rate–pressure product. In addition, the global LV ejection fraction measured with gated $C^{15}O$ PET in group B was significantly reduced (39% ± 16% [24%–59%] in group B vs. 66% ± 16% [46%–91%] in group A, $P < 0.01$). LV end-systolic volume in group B was significantly increased (31.4 ± 9.2 cm^3 in group B vs. 15.2 ± 9.4 cm^3 in group A, $P < 0.01$), and LV end-diastolic volume was also significantly increased (52.7 ± 10.2 cm^3 in group B vs. 41.7 ± 11.5 cm^3 in group A, $P < 0.05$). Increased end-systolic and end-diastolic volumes are also clearly visible in Figure 2. Systolic blood pressure and diastolic blood pressure, as well as rate–pressure product, were reduced during adenosine study in both groups. Heart rate was increased in group A but not in group B. Other parameters such as hemoglobin concentration (g/dL), percentage saturation of arterial O_2, $PaCO_2$ (mm Hg), and PO_2 (mm Hg) were not significantly different between the 2 groups. Table 2 shows detailed hemodynamic parameters [Table 2] and the results from the histologic analysis for each individual animal in group B. Wall motion score was reduced (akinesis–dyskinesis or 2–3) in the anterior wall, which includes the area of MI. The wall motion score was also reduced diffusely in all animals and indicated hypokinesis (grade 1) in the infarct-remote posterolateral wall. The coronary angiography demonstrated complete occlusion of the LAD in all animals in group B. As shown in Figure 4, no [Fig. 4] clear collateral circulation existed.

Imaging Results

The myocardial perfusion ($H_2{}^{15}O$) and metabolism (^{18}F-FDG) images at the mid ventricular plane and their corresponding slices after histochemical staining for the animals in group B are displayed in Figure 5. In all animals, clear [Fig. 5] signs of MI were detected in the anterior wall. The surface area of the MI was 13.7 ± 4.3 cm^2, which corresponded to 27% ± 9% of the whole left ventricle. Both PTF and ^{18}F-FDG images visually agreed well with the stained slices. Moreover, the ^{18}F-FDG images agreed well with the qualitative PTF images in all animals. The spatial distribution and size of the developed MI are visually reproducible

TABLE 1
Physiologic Parameters of Pigs at Time of PET

Parameter	Group A (control, $n = 7$)	Group B (old MI, $n = 7$)
Body weight (kg)	26 ± 2.4	41 ± 8.2
Heart rate (beats·min^{-1})	72 ± 22.4 (82 ± 21.4*)	52 ± 6.3† (53 ± 9.2)
Systolic blood pressure (mm Hg)	131 ± 22.1 (95 ± 22.4‡)	111 ± 18.3† (97 ± 15.0*)
Diastolic blood pressure (mm Hg)	92 ± 19.3 (49 ± 16.7‡)	74 ± 13.6† (57 ± 11.9‡)
Rate pressure product (mm Hg·min^{-1})	9,567 ± 3,616 (5,657 ± 3201‡)	5,732 ± 1,151† (4,445 ± 948*)
Wall thickness (posterior–lateral wall) (cm)	1.2 ± 0.1	1.6 ± 0.1‡
End-diastolic LV volume (mL)	41.7 ± 11.5	52.73 ± 10.2†
End-systolic LV volume (mL)	15.2 ± 9.4	31.4 ± 9.2*
LV ejection fraction (%)	66.0 ± 16.2	39.7 ± 16.9*
Hemoglobin concentration (g/dL)	13 ± 1.5	12 ± 0.9
Saturation of arterial O_2 (%)	99 ± 1.0	99 ± 0.6
pCO_2 (mm Hg)	39 ± 2.7	41 ± 2.8
pO_2 (mm Hg)	125 ± 20.1	141 ± 11.4

*$P < 0.01$.
†$P < 0.05$.
‡$P < 0.001$.
Data are mean ± SD. Values in parentheses are from administration of maximum dose of adenosine.

jnm084848-pm 24 ■ 4/15/11

TABLE 2
Hemodynamic Parameters of Pigs with Old MI (Group B)

Subject no.	BW (kg)	HR (beats·min^{-1})	SBP (mm Hg)	DBP (mm Hg)	RPP (mm Hg·min^{-1})	tHb (g/dL)	SAT (%)	pCO_2 (mm Hg)	pO_2 (mm Hg)	WM		WT (posterior–lateral wall)	EDV (mL)	ESV (mL)	EF (%)	LV surface area (cm^2)	MI surface area (cm^2)	DAF (%)
										Anterior wall	Posterior–lateral wall							
1	37	53	117	72	6,201	10.8	98.7	37.8	132	3	1	1.6	39.5	29.9	24.3	53.7	10.9	20.3
2	39	38	110	70	4,180	11.5	98.9	37	154.5	2	1	1.6	58.2	42.4	27.1	57	16.2	28.4
3	33	53	85	60	4,505	11.5	99.3	39.3	137.7	3	1	1.6	55.4	42.3	23.6	50	16	31.9
4	32	55	91	58	5,005	11.3	99.6	40.7	135.5	–	–	1.8	0	0	0	53.9	9.2	17.1
5	45	52	137	93	7,124	10.3	98.1	43.6	124.1	3	1	1.8	68.4	27.6	59.7	50	19.9	39.7
6	50	52	126	90	6,552	11.8	99.7	42.8	148.4	3	1	1.5	49.3	27.1	45	48.6	15.5	31.8
7	53	58	113	78	6,554	13.3	99	43.7	152.8	2	1	1.5	45.7	19.1	58.2	49.8	8.4	16.9
Mean	41	52	111	74	5,732	12	99	41	141	2.7	1	1.6	52.7	31.4	39.7	51.9	13.7	26.6
SD	8.2	6.3	18.3	13.6	1,151	0.9	0.6	2.8	11.4	0.5	0	0.1	10.2	9.2	16.9	3.05	4.3	8.7

BW = body weight; HR = heart rate; SBP = systolic blood pressure; DBP = diastolic blood pressure; RPP = rate–pressure product; tHB = hemoglobin concentration; SAT = saturation of arterial O_2; WM = wall motion; WT = wall thickness; EDV = end-diastolic LV volume; ESV = end-systolic LV volume; EF = ejection fraction; DAF = defect area fraction.

RGB

FIGURE 4. Example of coronary angiogram in animal with ameroid constrictor (arrow) (group B).

among the animals. Myocardial hypertrophy was visible in the wall regions remote from the infarcted area. In group B, the posterior–lateral wall thickness estimated from histochemical staining was 16 ± 1 mm (Table 2), which was significantly greater than that of group A (12 ± 1 mm; Table 1) ($P < 0.001$).

Further analysis of the size of the infarcted region is displayed in Figure 5B. We excluded 1 animal whose ^{18}F-FDG PET images demonstrated high accumulation at the anterior LV area (and therefore a smaller value in the defect surface area), which was attributed to the adhesion or inflammation between the myocardial and chest walls. Thus, the defect area on histology showed intersubject variation of approximately 20%. The results of both ^{18}F-FDG and PTF image analysis and histochemical analysis agreed well (Fig. 5B). Baseline and adenosine-stimulated MBF were also clearly blunted in the anterior wall in the animals in group B (Fig. 6A). Interestingly, abnormally reduced adenosine flow response also was detected in the myocardial regions remote from the MI in group B, whereas the baseline flow values were normal. [**Fig. 6**]

Further analysis of myocardial PTF and PTI values—indices of PTF—revealed that these values were significantly reduced in the infarcted anterior wall in group B (Fig. 6B). PTI was also moderately but significantly (~10%) reduced in the remote myocardial wall in group B.

Histologic Analysis

Histologic analysis did not show any signs of MI in group A, but transmural anterior wall MI was apparent in all animals in group B. Hypertrophy was detected in the posterior wall of group B in all animals. Multinuclear muscle cell breeding (Fig. 7A) and hyperplasia of blood vessels (Fig. 7B) were also visible in all animals in group B, mostly in the subendocardial regions. Denaturation necrosis with epicardial fibrous change and hypertrophy has also been seen in the lateral–posterior wall regions of group B (Fig. 7C). [**Fig. 7**]

DISCUSSION

This study demonstrated that 75% of pigs with old MI generated by the 2 steps of LAD ligation survived more than 4 mo. Such a long survival has never, to our

jnm084848-pm ■ 4/15/11

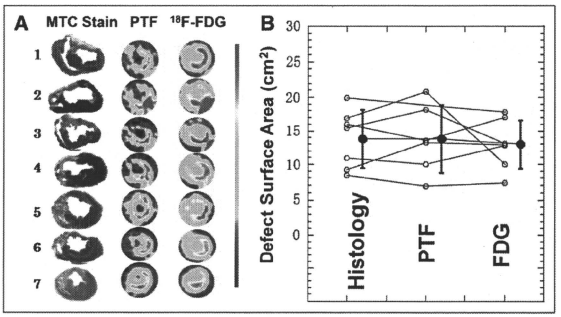

FIGURE 5. (A) Histologic, PTF, and ^{18}F-FDG slices at middle level of left ventricle in 7 animals of group B. Spatial distribution and size of MI are visually reproducible among animals. Myocardial hypertrophy was visible in remote myocardial wall regions. (B) Comparison of defect surface areas obtained from histologic stained slices with PET images using ^{18}F-FDG and PTF. MTC = Masson trichrome.

RGB

knowledge, been accomplished in any studies of pig heart disease. The size of MI reached approximately 27% of the whole left ventricle, causing the remodeling and global LV dilatation (significantly increased LV end-systolic and end-diastolic volumes) to be associated with reduced global LV function. PET with $C^{15}O$ and ^{18}F-FDG showed that regional LV wall motion was impaired not only in the infarcted region but also in the myocardial areas remote from the MI. PET also demonstrated reduced MBF reactivity in remote regions in addition to the infarct area. PTI was also reduced in the remote region, suggesting development of microscopic fibrosis. Moreover, other findings from histology indicated the existence of abnormalities in the noninfarcted area remote from the MI. These results indicate that this animal model may be close to human CHF after MI.

Shen et al. (*16*) adopted additional pacing tachycardia in pigs after sequential coronary artery ligations and observed global LV dysfunction, claiming that CHF was introduced. The present study is similar to the study by Shen et al. (*16*) but is based on only sequential coronary artery obstructions accomplished with acute distal coronary artery occlusion followed by a chronic proximal coronary occlusion with an ameroid constrictor, causing similar LV dysfunction. Of note was the better survival rate (80% at 1 mo, 75% at 4 mo) demonstrated in the current report than in any previous report (*6,8–12,14,16*), including Shen et al.

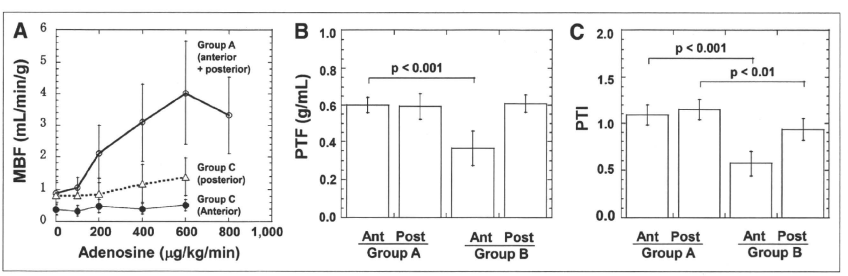

FIGURE 6. Results from PET studies. (A) Regional MBF as function of adenosine dose. In group A, MBF increases with increasing adenosine dose. In infarcted anterior wall of group B, MBF is reduced at rest and does not respond to adenosine. In posterior wall region, adenosine reactivity was significantly reduced. (B and C) Comparison of water-PTF (B) and water-PTI (C). Both were reduced in anterior wall of group B. PTI was also reduced in posterior wall in group B. Ant = anterior; Post = posterior.

jnm084848-pm 26 ■ 4/15/11

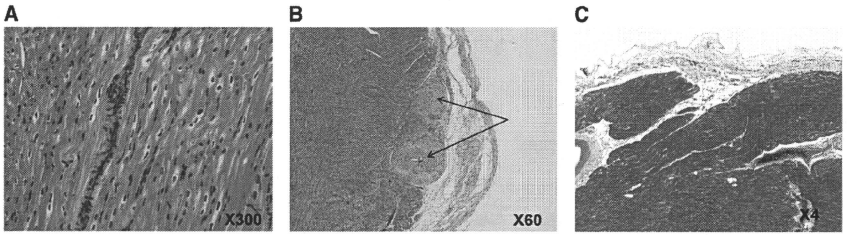

FIGURE 7. Typical images of histologic staining obtained from group B. Hypertrophy with multinuclear muscle cell breeding (A), hyperplasia of blood vessels shown as arrows (B), and denaturation necrosis often seen in subendocardial regions, as in this picture (C), are typical findings.

(73.3% at 21 d). In addition, it has not been confirmed whether such a good survival rate at 21 d could last more than 4 mo after producing global LV dysfunction with MI. Our preliminary experiment, independently performed on 69 farm pigs, demonstrated that when the proximal LAD was occluded by the ameroid constrictor alone, 45 pigs (65%) died within a month, and the total survival rate was 30% at 4 mo. This survival rate is significantly smaller than the rates from the present study.

The reason why animals with MI acquired such good survival is not fully understood. However, it was clearly observed that the ligation of the peripheral coronary artery before the gradual occlusion of the main trunk of the LAD apparently inhibited the fibrillation during the operation. This procedure is obviously effective at protecting against fatal arrhythmias. This preconditioning effect is supported by the experiments of Moses et al. (*27*), in which ischemic preconditioning of the distal coronary artery protected cardiac muscle through a mechanism involving the potassium channels of mitochondria and myocytes. There may be contributions from other preconditioning factors (*9,28–30*) that associate with increased tolerance of ischemia. Another mechanism could be associated with the modulation of sympathetic tone. It has been reported that regional heterogeneity in myocardial cellular mechanisms (responsible for myocardial cellular depolarization) and repolarization in hibernating myocardium (*12*) can induce ventricular fibrillation (*9*). Inhibition of such heterogeneous myocardial cellular mechanisms or control of modulated sympathetic tone could be another possible explanation.

The present study used a gradual total occlusion of the proximal of LAD, as evidenced by the coronary angiography (Fig. 4), and thus caused an MI of approximately 27% of the total myocardium. The global LV ejection fraction in group B was significantly reduced (39% vs. 66% in controls), showing that LV systolic function was impaired in group B. Both histology and PET had concordant findings. The baseline MBF in the MI area was reduced and was not responding to adenosine administration. This finding is reasonable because the infarcted tissue should have reduced capillary density, and the resistive vessels do not respond to any vasodilating stimulation. The physical extent and size of the MI were reproducible among the individual animals. This feature is important when this animal model is applied to evaluate various new pharmaceuticals or various regenerative therapeutic trials.

The noninfarcted myocardium developed clear signs of remodeling, such as hypokinesis, hypertrophy, and the accumulation of fibrotic tissue in the remote myocardial wall, and significantly decreased PTI values, a marker of residual fractionation of water-perfusable tissue. The baseline MBF was preserved, but reactivity to the adenosine was blunted, even at a maximum dose of 600 μg/kg/min. This reduced reactivity could be related to the degeneration of small arteries, possibly caused by enlargement of myocytes and development of moderate denaturation necrosis and fibrosis.

This study demonstrated that physiologic status and physical extent of MI can be evaluated using the noninvasive technique of PET. The defect surface area identified with ^{18}F-FDG was identical to that identified with PTF, and both agreed well with the results of histology. Furthermore, microscopic degeneration can be characterized as reduced reactivity of quantitative myocardial perfusion to adenosine. The PET-derived PTI, which is known to indicate the absolute fraction of non–scar tissue within the area (*22*), was reduced not only in the infarcted anterior wall but also in the remote region by 10%. As demonstrated in recent studies (*31–34*), the reduced PTI in a control region is thought to be caused by the development of microscopic fibrosis.

In this study, left-atrial and LV pressure analyses have not been measured, because the aims of this study were to create a long-survival pig model of MI and global LV dysfunction with remodeling, characterize this model using PET, and compare these parameters with histology before making a complete model of CHF after MI in pigs. One limitation of this study was that, because of technical reasons in our laboratory at the initiation of this study, it was difficult to measure left-atrial and LV pressures.

jnm084848-pm 27 ■ 4/15/11

CONCLUSION

Our pig model of postinfarction global LV dysfunction was characterized by a high survival rate and large MI, with clear signs of cardiac remodeling, as demonstrated by PET and histology. This animal model might contribute to investigations of MI and new therapies for cardiac remodeling in MI.

ACKNOWLEDGMENTS

We thank the staff of the Department of Investigative Radiology of National Cardiovascular Center for invaluable technical assistance. This study was supported by a research grant from New Energy and Industrial Technology Development Organization (NEDO), Japan, and grants for translational research and nanomedicine from the Ministry of Health, Labor and Welfare (MHLW), Japan.

REFERENCES

1. Saito I, Folsom AR, Aono H, Ozawa H, Ikebe T, Yamashita T. Comparison of fatal coronary heart disease occurrence based on population surveys in Japan and the USA. *Int J Epidemiol.* 2000;29:837–844.
2. Balady GJ, Jette D, Scheer J, Downing J. Changes in exercise capacity following cardiac rehabilitation in patients stratified according to age and gender: results of the Massachusetts Association of Cardiovascular and Pulmonary Rehabilitation Multicenter Database. *J Cardiopulm Rehabil.* 1996;16:38–46.
3. Krum H, Haas SJ, Eichhorn E, et al. Prognostic benefit of beta-blockers in patients not receiving ACE-inhibitors. *Eur Heart J.* 2005;26:2154–2158.
4. Anversa P, Leri A, Kajstura J. Cardiac regeneration. *J Am Coll Cardiol.* 2006;47:1769–1776.
5. Gheeraert PJ, Henriques JP, De Buyzere ML, De Pauw M, Taeymans Y, Zijlstra F. Preinfarction angina protects against out-of-hospital ventricular fibrillation in patients with acute occlusion of the left coronary artery. *J Am Coll Cardiol.* 2001;38:1369–1374.
6. Millard RW. Induction of functional coronary collaterals in the swine heart. *Basic Res Cardiol.* 1981;76:468–473.
7. Roth DM, Maruoka Y, Rogers J, White FC, Longhurst JC, Bloor CM. Development of coronary collateral circulation in left circumflex Ameroid-occluded swine myocardium. *Am J Physiol.* 1987;253:H1279–H1288.
8. Fallavollita JA, Riegel BJ, Suzuki G, Valeti U, Canty JM Jr. Mechanism of sudden cardiac death in pigs with viable chronically dysfunctional myocardium and ischemic cardiomyopathy. *Am J Physiol Heart Circ Physiol.* 2005;289:H2688–H2696.
9. Canty JM Jr, Suzuki G, Banas MD, Verheyen F, Borgers M, Fallavollita JA. Hibernating myocardium: chronically adapted to ischemia but vulnerable to sudden death. *Circ Res.* 2004;94:1142–1149.
10. Fallavollita JA, Canty JM Jr. Differential ^{18}F-2-deoxyglucose uptake in viable dysfunctional myocardium with normal resting perfusion: evidence for chronic stunning in pigs. *Circulation.* 1999;99:2798–2805.
11. Fallavollita JA, Canty JM Jr. Ischemic cardiomyopathy in pigs with two-vessel occlusion and viable, chronically dysfunctional myocardium. *Am J Physiol Heart Circ Physiol.* 2002;282:H1370–H1379.
12. Fallavollita JA, Logue M, Canty JM Jr. Stability of hibernating myocardium in pigs with a chronic left anterior descending coronary artery stenosis: absence of progressive fibrosis in the setting of stable reductions in flow, function and coronary flow reserve. *J Am Coll Cardiol.* 2001;37:1989–1995.
13. Shen YT, Vatner SF. Mechanism of impaired myocardial function during progressive coronary stenosis in conscious pigs: hibernation versus stunning? *Circ Res.* 1995;76:479–488.
14. Mills I, Fallon JT, Wrenn D, et al. Adaptive responses of coronary circulation and myocardium to chronic reduction in perfusion pressure and flow. *Am J Physiol.* 1994;266:H447–H457.
15. Roth DM, White FC, Nichols ML, Dobbs SL, Longhurst JC, Bloor CM. Effect of long-term exercise on regional myocardial function and coronary collateral development after gradual coronary artery occlusion in pigs. *Circulation.* 1990;82:1778–1789.
16. Shen YT, Lynch JJ, Shannon RP, Wiedmann RT. A novel heart failure model induced by sequential coronary artery occlusions and tachycardiac stress in awake pigs. *Am J Physiol.* 1999;277:H388–H398.
17. *Guide for the Care and Use of Laboratory Animals.* Washington, DC: National Academy Press; 1996.
18. O'Konski MS, White FC, Longhurst J, Roth D, Bloor CM. Ameroid constriction of the proximal left circumflex coronary artery in swine: a model of limited coronary collateral circulation. *Am J Cardiovasc Pathol.* 1987;1:69–77.
19. Iida H, Takahashi A, Tamura Y, Ono Y, Lammertsma AA. Myocardial blood flow: comparison of oxygen-15-water bolus injection, slow infusion and oxygen-15-carbon dioxide slow inhalation. *J Nucl Med.* 1995;36:78–85.
20. DeFronzo RA, Tobin JD, Andres R. Glucose clamp technique: a method for quantifying insulin secretion and resistance. *Am J Physiol.* 1979;237:E214–E223.
21. Knuuti MJ, Nuutila P, Ruotsalainen U, et al. Euglycemic hyperinsulinemic clamp and oral glucose load in stimulating myocardial glucose utilization during positron emission tomography. *J Nucl Med.* 1992;33:1255–1262.
22. Iida H, Tamura Y, Kitamura K, Bloomfield PM, Eberl S, Ono Y. Histochemical correlates of ^{15}O-water-perfusable tissue fraction in experimental canine studies of old myocardial infarction. *J Nucl Med.* 2000;41:1737–1745.
23. Iida H, Rhodes CG, de Silva R, et al. Myocardial tissue fraction: correction for partial volume effects and measure of tissue viability. *J Nucl Med.* 1991;32:2169–2175.
24. Iida H, Rhodes CG, de Silva R, et al. Use of the left ventricular time-activity curve as a noninvasive input function in dynamic oxygen-15-water positron emission tomography. *J Nucl Med.* 1992;33:1669–1677.
25. de Silva R, Yamamoto Y, Rhodes CG, et al. Preoperative prediction of the outcome of coronary revascularization using positron emission tomography. *Circulation.* 1992;86:1738–1742.
26. Yamamoto Y, de Silva R, Rhodes CG, et al. A new strategy for the assessment of viable myocardium and regional myocardial blood flow using ^{15}O-water and dynamic positron emission tomography. *Circulation.* 1992;86:167–178.
27. Moses MA, Addison PD, Neligan PC, et al. Inducing late phase of infarct protection in skeletal muscle by remote preconditioning: efficacy and mechanism. *Am J Physiol Regul Integr Comp Physiol.* 2005;289:R1609–R1617.
28. Kitakaze M, Node K, Minamino T, et al. Role of activation of protein kinase C in the infarct size-limiting effect of ischemic preconditioning through activation of ecto-5′-nucleotidase. *Circulation.* 1996;93:781–791.
29. Kharbanda RK, Mortensen UM, White PA, et al. Transient limb ischemia induces remote ischemic preconditioning in vivo. *Circulation.* 2002;106:2881–2883.
30. Chen PS, Chen LS, Cao JM, Sharifi B, Karagueuzian HS, Fishbein MC. Sympathetic nerve sprouting, electrical remodeling and the mechanisms of sudden cardiac death. *Cardiovasc Res.* 2001;50:409–416.
31. Knaapen P, Boellaard R, Gotte MJ, et al. Perfusable tissue index as a potential marker of fibrosis in patients with idiopathic dilated cardiomyopathy. *J Nucl Med.* 2004;45:1299–1304.
32. Knaapen P, Boellaard R, Gotte MJ, et al. The perfusable tissue index: a marker of myocardial viability. *J Nucl Cardiol.* 2003;10:684–691.
33. Knaapen P, Bondarenko O, Beek AM, et al. Impact of scar on water-perfusable tissue index in chronic ischemic heart disease: evaluation with PET and contrast-enhanced MRI. *Mol Imaging Biol.* 2006;8:245–251.
34. Knaapen P, van Dockum WG, Bondarenko O, et al. Delayed contrast enhancement and perfusable tissue index in hypertrophic cardiomyopathy: comparison between cardiac MRI and PET. *J Nucl Med.* 2005;46:923–929.

28
jnm084848-pm ■ 4/15/11

Sex Differences in Patients With Asymptomatic Carotid Atherosclerotic Plaque

In Vivo 3.0-T Magnetic Resonance Study

Hideki Ota, MD, PhD; Mathew J. Reeves, BVSc, PhD; David C. Zhu, PhD; Arshad Majid, MD; Alonso Collar, MD, FACS; Chun Yuan, PhD; J. Kevin DeMarco, MD

Background and Purpose—Stroke prevention with carotid endarterectomy in asymptomatic men with carotid stenosis is greater than in women. Men have a higher incidence of stroke <75 years of age. Sex differences in plaque characteristics may help explain this, because several plaque features, including a thin/ruptured fibrous cap, larger lipid-rich/necrotic core, and hemorrhage, are associated with increased risk of stroke. We hypothesize that MRI carotid plaque features will demonstrate sex differences indicative of higher-risk plaque in men.

Methods—One hundred thirty-one patients (men, 67; women, 64) with ≥50% asymptomatic carotid stenosis on duplex ultrasound were included. Two blinded reviewers interpreted multicontrast MRI. Presence of a thin/ruptured fibrous cap, plaque components (lipid-rich/necrotic core, hemorrhage, and calcification), and percent component volume were documented. The associations between sex and individual plaque characteristics were examined using logistic and linear regression models (2-part models) controlling for demographic characteristics and MR angiographic findings.

Results—Presence of a thin/ruptured fibrous cap (48% versus 17%, adjusted OR=4.41, $P<0.01$) and lipid-rich/necrotic core (73% versus 50%, adjusted OR=3.66, $P=0.01$) were more common in men. There was a trend for more highly prevalent hemorrhage (33% versus, 17%, adjusted OR=2.15, $P=0.07$) in men. Calcification was not significantly associated with sex. Men demonstrated larger volumes of percent lipid-rich/necrotic core (median, 7.7% versus 3.2%, $P=0.01$), and percent hemorrhage (median, 6.1% versus 1.5%, $P<0.01$).

Conclusion—In patients with asymptomatic ≥50% carotid stenosis by duplex ultrasound, men had higher-risk plaque features compared with women after controlling for potential confounders. These findings may help explain sex differences in stroke incidence and prevention. **(*Stroke*. 2010;41:1630-1635.)**

Key Words: atherosclerosis ■ magnetic resonance imaging ■ sex

In a recent heart disease and stroke statistics update, the stroke incidence rate was noted to be higher in men compared with women age <75 years.[1] Carotid endarterectomy (CEA) to prevent future stroke in asymptomatic patients with carotid stenosis is more beneficial in men than women.[2] For men, the relative risk reduction from CEA was 51% (relative risk 0.49, 95% CI 0.36 to 0.66), but for women it was only 4% (relative risk 0.96, 95% CI, 0.64 to 1.44).[2]

The exact causes or mechanisms for the sex differences in stroke incidence rate in patients <75 years of age and CEA outcomes are not fully understood. Because plaque rupture is a common precipitating event for thromboembolic events,[3–5] CEA to remove atherosclerotic plaque prone to rupture should result in reduced clinical events. Recent work has demonstrated the ability of in vivo MR images to identify "high-risk" carotid plaque features that are associated with subsequent stroke or transient ischemic attack thought to be due to plaque rupture.[6,7] Variations in these MR identified "high-risk" carotid plaque features may help explain sex differences in stroke incidence and prevention.

To our knowledge, only a few studies have examined sex differences in plaque morphology. In a study using carotid artery duplex ultrasound (DUS), Iemolo et al scanned 1686 patients recruited with vascular disease, stroke, transient ischemic attack, or asymptomatic carotid stenosis and followed them for up to 5 years; men were shown to have less carotid stenosis but more plaque area than women.[8] Carotid plaque area was found to be a stronger predictor of stroke risk than stenosis in this study. A study that used histological analysis of CEA specimens revealed several significant sex differences, including frequent atheromatous plaques (containing >40% fat), higher macrophage staining, weaker

Received February 23, 2010; final revision received April 22, 2010; accepted May 20, 2010.

From the Departments of Radiology (H.O., D.C.Z., J.K.D.), Epidemiology (M.J.R.), and Neurology and Ophthalmology (A.M.), Michigan State University, East Lansing, Mich; Ingham Cardiothoracic & Vascular Surgeons (A.C.), Lansing, Mich; and the Department of Radiology (C.Y.), University of Washington, Seattle, Wash.

Correspondence to J. Kevin DeMarco, MD, Michigan State University, Department of Radiology, 184 Radiology Building, East Lansing, MI 48824-1313. E-mail jkd@rad.msu.edu

***Stroke* is available at http://stroke.ahajournals.org** **DOI: 10.1161/STROKEAHA.110.581306**

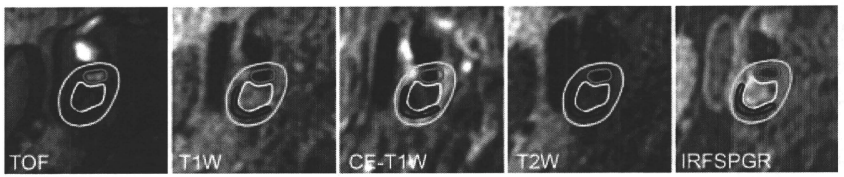

Figure 1. An example of images with overlays by MRI—plaque view. Red indicates luminal boundary; light blue, outer wall boundary; the area outlined by yellow appears iso- to hyperintense on T1-weighted image and hypoenhanced on contrast-enhanced T1-weighted image indicating LR/NC; the area inside black line appears hypointense on all the images, indicating calcification. TOF indicates time of flight; T1W, T1-weighted; CE-T1W, contrast-enhanced T1-weighted; IRFSPGR, inversion recovery fast spoiled gradient recalled.

smooth muscle cell staining, higher plaque concentration of interleukin-8, and higher matrix metalloproteinase-8 activity in men compared with women.[9] The results of this study indicated that men had more unstable carotid plaque that included more features of inflammation compared with women.[9]

In vivo carotid MRI has the ability to visualize atherosclerotic plaque components such as a lipid-rich/necrotic core (LR/NC), calcification, intraplaque hemorrhage, and fibrous cap status and has been shown to have good concordance with histology.[10–16] Previous MRI-based studies of carotid lesions demonstrated that a large LR/NC, thin/ruptured fibrous cap, intraplaque hemorrhage, and larger maximal wall thickness were associated with a higher risk of cerebrovascular ischemic events in patients with >50% stenosis on DUS.[6,7,17] However, to our knowledge, there have been no previous studies examining sex differences for carotid plaque characteristics evaluated by in vivo MRI.

The aim of this study was to test the hypothesis that carotid plaque features detected by in vivo MRI demonstrate sex differences indicative of higher-risk plaque in men compared with women in asymptomatic patients referred to subspecialists for the evaluation of >50% carotid stenosis identified on DUS or CT angiogram.

Materials and Methods

The study procedures were approved by the Community Research Institutional Review Board at Michigan State University and informed consent was obtained from all patients.

Subjects

Between March 2006 and July 2009, 208 patients (119 men, 89 women) were referred to the Department of Radiology, Michigan State University, East Lansing, Mich, for evaluation of asymptomatic moderate or severe carotid stenosis by 3-T MRI. Ninety percent were referred from a vascular interventional clinic with the remainder from either neurology or cardiology outpatient services. The vascular surgeons, neurologists, and cardiologist approached all of their patients with documented asymptomatic carotid stenosis about participation in this study. Inclusion criteria were: (1) 50% to 99% carotid stenosis as measured by DUS or CT angiography on at least 1 side; (2) no history of stroke, transient ischemic attack, or amorous fugax in the distribution of either carotid artery within 4 months before enrollment; and (3) no contraindications for MRI. Baseline clinical characteristics, including sex, age, race, body mass index, and history of hyperlipidemia, hypertension, diabetes, coronary artery disease, peripheral artery disease, statin use, and smoking, were collected by the referring physicians.

MRI Protocol

Patients were imaged with a 3-T whole-body scanner (Signa Excite; GE Healthcare, Waukesha, Wis) and a 4-channel phased-array surface coil (Pathway MRI, Seattle, Wash). The plaque multicontrast imaging protocol included the following 5 sequences: 3-dimensional time-of-flight, precontrast T1-weighted, T2-weighted, 3-dimensional inversion recovery fast spoiled gradient recalled,[18] and contrast-enhanced T1-weighted performed 5 minutes after intravenous infusion of 0.15 mmol gadobenate dimeglumine (Multihance; Bracco Diagnostic Inc, Princeton, NJ) per kilogram of body weight at a rate of 3 mL/s. The 5 sequences were obtained based on previously published protocols for a 3.0-T scanner.[18,19] Details of MRI parameters were demonstrated in Supplemental Table I(available at http://stroke.ahajournals.org). After intravenous bolus contrast injection, very high (0.28 mm^3), resolution coronal elliptical-centric carotid contrast-enhanced MR angiogram was performed with a test bolus to time the contrast arrival time.[20] Approximate scan time including patient preparation was 45 minutes.

MRI Image Review and Criteria

Before the image review, the more severely stenotic side as previously determined by DUS or CT angiography was assigned as the index carotid artery. Each patient contributed only 1 set of observations (ie, the index carotid artery) to the data set for analysis. Two experienced reviewers who were blinded to clinical outcome reviewed all MR images, and a consensus decision was reached for each plaque feature as has been previously described.[6] The quality of the overall images was scored using an image quality score rated on a 4-point scale (1=poor, 4=excellent). Arteries with an average image quality=1 were excluded from the study.[19]

The extracranial carotid bifurcation level was used as a landmark for matching the 5 different weightings. Areas of the lumen, wall, and plaque components (LR/NC, intraplaque hemorrhage, and calcification) were manually outlined (Figure 1). These plaque components were identified based on histologically validated criteria.[10–16] When a LR/NC was identified, the fibrous cap status was categorized as either a "thick" or "thin/ruptured" fibrous cap using histologically validated criteria.[11,16] Details of criteria are demonstrated in Supplemental Table II. Area measurements were obtained using an imaging analysis tool for carotid plaque MRI (MRI-Plaque View; VP Diagnostics, Seattle, Wash). This software allows: (1) to display simultaneously all the matched slices; (2) to provide in-plane registration and boundary identification so that signals inside the contours can be easily recognized; and (3) to produce a comprehensive lesion report, including sizes of the plaque components as well as the vessel wall. For plaque composition, the proportion of wall volume occupied by that feature was calculated for each artery (percent volume). This calculation normalizes compositional features to the vessel size to account for the innate differences in arterial size between subjects.

Lastly, 2 experienced reviewers, blinded to clinical information and carotid plaque findings, evaluated the level and degree of stenosis. The measurement of percent diameter carotid stenosis was based on the North American Symptomatic Carotid Endarterectomy

Trial criteria,[21] using the high-resolution carotid contrast-enhanced MR angiogram on multiplanar reformations generated using a 3-dimensional workstation (Advantage Windows version 4.3; GE Healthcare, Waukesha, Wis).

Statistical Analysis

Descriptive frequencies for categorical variables and means and medians (interquartile range) for continuous variables were generated for the overall population and for each sex. Sex differences in baseline clinical characteristics and MR angiographic findings were tested using χ^2 analysis or t tests. A logistic regression analysis was used to compare fibrous cap status (presence or absence of thin/ruptured fibrous cap) between sexes. A 2-part model[22] was fit to examine sex differences in the presence and size of the other plaque components, including LR/NC, intraplaque hemorrhage, and calcification. In the first part of this model, the presence/absence of a plaque component was evaluated using logistic regression analysis. In the second part, only subjects with values for component volumes (ie, values >0) are modeled using linear regression analysis. Natural log transformations were performed for all percent volume data because it was positively skewed.

Baseline characteristics demonstrating an association with sex ($P<0.20$) were considered as potential confounding factors and included in subsequent multivariable analyses. Variables were selected into the final multivariate model using a stepwise backward selection method ($P>0.10$ for removal from model). Results were expressed as adjusted OR (aOR) with 95% CIs for logistic regression models and as regression coefficients with 95% CIs for linear regression models. The regression coefficients from the linear models indicate the increase in the log percent volume in men versus women for each component. $P<0.05$ was used to designate statistical significance in the multivariate models. Computation was performed using SPSS Version 17.0 (SPSS, Chicago, Ill).

Results

Of the 208 patients initially referred for possible inclusion in this study, all had documented 50% to 99% carotid stenosis of at least 1 side by DUS or CT angiography within the past 6 months. A total 70 patients did not meet the inclusion criteria. Specifically, 7 women and 21 men were too obese/claustrophobic; 8 women and 16 men had implanted devices such as vascular stents or pacemakers that were not approved for 3-T MRI; 5 women and 9 men declined to participate in the study; 2 women and 1 man had chronic obstructive pulmonary disease or congestive heart failure that precluded their ability to lay flat for imaging; and 1 man was excluded for other reasons. Therefore, a total of 138 patients met all the inclusion and exclusion criteria.

Seven of these 138 patients with an average image quality score of 1 across all cross-sections were excluded. The remaining 131 patients consisted of 67 men (mean±SD age, 70.1±8.6 years) and 64 women (69.4±8.9 years).

Table 1 illustrates the baseline clinical characteristics and MR angiographic findings in the 131 patients. These patients demonstrated high prevalence of traditional risk factors for cerebrovascular diseases (Table 1). Prevalence of coronary artery disease was significantly higher in men than women ($P=0.02$). Although not statistically significant, higher body mass index, lower prevalence of hyperlipidemia, higher prevalence of statin use, and higher MR angiographic stenosis were seen in men compared with women ($P<0.20$). These 5 variables were therefore selected as potential confounders in the multivariable models.

Table 1. Baseline Clinical Characteristics, Degree of MR Angiographic Stenosis, and Level of Stenosis in Men and Women

Variable	Men (n=67)	Women (n=64)	P
Age, years	70.1±8.6*	69.4±8.9*	0.40
White patients, %	94	89	0.36
Body mass index, kg/m^2	28.3±4.5*	27.0±4.9*	0.11†
Hyperlipidemia, %	72	83	0.13†
Hypertension,%	73	78	0.51
History of coronary artery disease, %	48	28	0.02†
History of peripheral vascular disease, %	21	27	0.45
History of diabetes mellitus, %	22	19	0.61
Current statin use, %	87	75	0.10†
Ever smoked, %	74	65	0.35
Current	25	21	0.64
Past	49	44	0.53
Never	25	34	0.41
MR angiographic degree of stenosis	64.1±21.9*	58.9±18.9*	0.12†
Level of stenosis			
Common carotid, %	9	13	0.58
Carotid bulb, %	46	48	0.86
Internal carotid, %	45	39	0.60

*Mean±SD.

†Variables with $P<0.20$ were selected as potential confounders in the multivariate models.

For the presence of a thin/ruptured fibrous cap, ORs in the univariate and multivariable models remained unchanged because none of the 5 potential confounders remained in the final model. For the presence of LR/NC, statin use (aOR=0.12, 95%CI=0.03 to 0.45, $P=0.02$) was included in the final multivariable model. For the presence of hemorrhage, the MR angiographic degree of stenosis (aOR for 10% increase=1.22, 95%CI=0.98 to 1.51, $P=0.08$) was included in the final multivariable model.

The prevalence of thin/ruptured fibrous cap and LR/NC were significantly higher in men than women (Table 2). In multivariate logistic regression analyses, aORs were 4.41 (95% CI=1.97 to 9.87, $P<0.01$) for the presence of thin/ruptured fibrous cap and 3.66 (95% CI=1.67 to 8.00, $P=0.01$) for the presence of LR/NC (Figures 2 and 3). Although men had a significantly higher prevalence of hemorrhage in the univariate model, this was only marginally significant in the multivariate model (aOR=2.15, 95% CI=0.93 to 4.98, $P=0.07$), although the magnitude of OR changed little from the univariate analysis (2.36).

When subjects having individual plaque components were examined, median (25th, 75th percentile), percent component volumes in men and women were 7.66% (2.40%, 19.90%) versus 3.23% (1.15%, 6.89%) for LR/NC, 6.13% (1.97%, 10.81%) versus 1.49% (0.67%, 2.52%) for hemorrhage, and 3.13% (1.20%, 7.09%) versus 3.29% (1.52%, 6.69%) for calcification, respectively. Median with 25th and 75th of log

Table 2. Prevalence and Percent Volume of Plaque Components in Men and Women: Univariate and Multivariable

			Univariate Model			Multivariable Model		
Presence	Men, %	Women, %	OR	95% CI	P	aOR	95% CI	P
Thin/ruptured fibrous cap	48	17	4.41	1.97–9.87	<0.01	4.41*	1.97–9.87	<0.01
LR/NC	73	50	2.72	1.31–5.65	0.01	3.66†	1.67–8.00	0.01
Hemorrhage	33	17	2.36	1.03–5.38	0.04	2.15‡	0.93–4.98	0.07
Calcification	84	86	0.83	0.32–2.17	0.71	0.66‡	0.24–1.81	0.41
Log (Percent Volume)	Median (25th, 75th)	Median (25th, 75th)	Coefficient	95% CI	P	Coefficient	95% CI	P
LR/NC (n=81)	2.04 (0.87–2.99)	1.17 (0.37–1.93)	0.79	0.23–1.36	<0.01	0.71‡	0.17–1.25	0.01
Hemorrhage (n=33)	1.81 (0.66–2.38)	0.40 (−0.40–0.92)	1.47	0.63–2.31	<0.01	1.47*	0.63–2.31	<0.01
Calcification (n=111)	1.14 (0.18–1.96)	1.19 (0.42–1.90)	−0.04	−0.48–0.40	0.86	−0.16‡	−0.58–0.26	0.45

OR or aOR by logistic regression analyses. Coefficients for log (percent volume) of patients with presence of individual plaque components by linear regression analyses.

Models also include: *none; †statin use; ‡MR angiographic degree of stenosis.

percent volumes for LR/NC, hemorrhage, and calcification in men and women are demonstrated in Table 2. The size of LR/NC and hemorrhage were both significantly larger in men than women in both univariate and multivariable models (Table 2).

For log percent LR/NC, the MR angiographic degree of stenosis (coefficient for 10% increase=0.18, 95% CI=0.06 to 0.30, P=0.01) was included as a potential confounder in the final multivariable model. For log percent hemorrhage, none of the 5 potential confounders remained in the final model.

Neither presence nor size of calcification was significantly different between men and women. In multivariate models, MR angiographic degree of stenosis was significantly associated with both the presence of calcification (aOR for 10% increase=1.28, 95% CI=1.03 to 1.59, P=0.03) and log percent calcification (coefficient for 10% increase=0.21, 95% CI=0.10 to 0.32, P<0.01).

Discussion

To our knowledge, this is the first study to reveal that carotid plaque characteristics identified by 3-T in vivo MRI differ between men and women who are referred to subspecialists for the evaluation of asymptomatic carotid stenosis seen on DUS or CT angiogram. Men tend to have carotid plaque characterized by the presence of LR/NC and thin/ruptured fibrous cap as well as larger percent volume of LR/NC and intraplaque hemorrhage as compared with women.

We determined baseline patient characteristics and MR angiographic findings as potential confounders to characterize plaque features. It is known that the prevalence of intraplaque hemorrhage is high in CEA specimens removed from severely stenotic carotid arteries,[23] and the prevalence of complicated American Heart Association Type VI carotid atherosclerotic lesions increases as the degree of stenosis increases from 1% to 15% to 80% to 99%.[24] The present study demonstrated that LR/NC and a thin/ruptured fibrous cap occurred more often in men than women even after adjusting for potential confounders. Presence of hemorrhage was also higher in men but only reached marginal significance in the multivariable analysis.

Atherosclerotic plaque that is prone to rupture because of its intrinsic composition such as intraplaque hemorrhage and a large lipid core[3–5] are associated with subsequent thromboembolic ischemic events. Takaya and colleagues used 1.5-T MRI to demonstrate that presence of a thin/ruptured fibrous cap, the presence and size of intraplaque hemorrhage, the size of LR/NC, and larger wall thickness were associated with subsequent cerebrovascular events.[6] Singh et al demonstrated MR-depicted intraplaque hemorrhage was associated with future ipsilateral cerebrovascular events.[7] Both of these studies included mostly male subjects (ie, 82% and 100%, respectively) and so did not include sex-specific analyses.

In a study of 450 consecutive patients undergoing CEA, Hellings et al demonstrated that asymptomatic women had

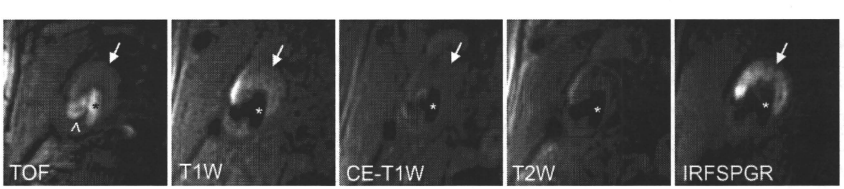

Figure 2. A representative case of large hemorrhagic LR/NC with a ruptured fibrous cap obtained from a male patient. Irregular luminal surface with protruding hyperintensity area on time of flight indicates fibrous cap rupture/ulceration (chevron). Area with hypointensity on contrast-enhanced T1-weighted and hyperintensity on inversion recovery fast spoiled gradient recalled indicates a hemorrhagic lipid-rich/necrotic core (arrows). *Lumen. TOF indicates time of flight; T1W, T1-weighted; CE-T1W, contrast-enhanced T1-weighted; IRFSPGR, inversion recovery fast spoiled gradient recalled.

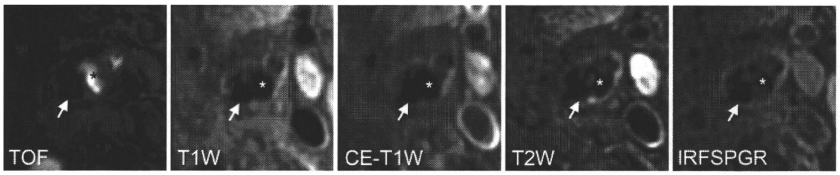

Figure 3. A representative case of calcified plaque from a female patient. Hypointensity area seen on all the images (arrows) indicates calcified plaque. *Lumen. TOF indicates time of flight; T1W, T1-weighted; CE-T1W, contrast-enhanced T1-weighted; IRFSPGR, inversion recovery fast spoiled gradient recalled.

the highest prevalence of stable plaque as determined by histological grading of plaque phenotype and biochemical features of unstable carotid plaque.[9] The results of our study are in agreement with these results and demonstrate a previously undescribed higher prevalence of a thin/ruptured fibrous cap and larger intraplaque hemorrhage in men compared with women. Previous authors have stressed the importance of corroborating these histological sex differences in preoperative testing or imaging of high-risk patients. The present results suggest that in vivo 3-T carotid plaque MRI can identify plaque phenotypes that are suggestive of high-risk patients or lesions. The increased incidence of these potentially "high-risk" carotid plaque phenotypes in men compared with women may be one reason that CEA is more effective in reducing subsequent stroke in asymptomatic men with carotid stenosis than women and is consistent with prior studies demonstrating a higher incidence of stroke in men than women age <75 years. These hypotheses would need to be tested in larger, prospective studies.

This study involved a selected group of patients with moderate to severe stenosis identified on their screening DUS or CT angiogram who were referred to subspecialists for further evaluation. Baseline characteristics in the present study appeared to be similar to those in previous CEA clinical trials and clinical studies of patients referred to vascular surgeons om which patients already have carotid stenosis[6,9,25,26] but demonstrated higher prevalence of risk factors compared with other general populations.[27] Although the present results may not be applicable to the general population, they would be applicable to clinical populations who undergo assessment for surgical treatment of carotid atherosclerotic disease.

This study has 2 major limitations. First, this is a cross-sectional study and so we were not able to demonstrate a direct association between plaque characteristics and subsequent stroke risk. Future prospective studies of noninvasive in vivo MRI are required to evaluate the role of sex-specific differences in plaque characteristics and their relationship to subsequent clinical events. Second, this is a single-center study. The results will need to be replicated in a multicenter study.

Summary

In patients with asymptomatic ≥50% carotid stenosis on the entry DUS or CT angiogram, carotid plaque characteristics differed by sex; men tended to have higher-risk plaque features compared with women. These findings may indicate a possible reason for why CEAs are more effective in asymptomatic men than women and why men age <75 years have a higher incidence of stroke than women. These results suggest the potential for the sex-specific management for patients with carotid atherosclerosis based on different plaque features. These results also suggest the need to undertake future prospective studies to determine the association between sex-specific plaque features and the risk of subsequent cerebrovascular events.

Acknowledgments

We thank our research technologists, Ms Colleen A. Hammond and Scarlett R. Doyle, for their help in acquiring the MR images.

Sources of Funding

Supported by American Heart Association Midwest Affiliate Grant-in-Aid 0855604G, Michigan State University/Office of Vice-President for Research & Graduate Studies, and the Office of the Provost through the Internal Grant Program 05-IRGP-472.

Disclosures

J.K.D. received support from GE Medical Systems; Honoraria from Bracco Diagnostic Inc; and served on an Advisory Board for GE Medical Systems. D.C.Z. received support from GE Medical Systems. GE had no role in any aspect of the conduct of this research. There are no other conflicts to report.

References

1. Lloyd-Jones D, Adams RJ, Brown TM, Carnethon M, Dai S, De Simone G, Ferguson TB, Ford E, Furie K, Gillespie C, Go A, Greenlund K, Haase N, Hailpern S, Ho PM, Howard V, Kissela B, Kittner S, Lackland D, Lisabeth L, Marelli A, McDermott MM, Meigs J, Mozaffarian D, Mussolino M, Nichol G, Roger VL, Rosamond W, Sacco R, Sorlie P, Stafford R, Thom T, Wasserthiel-Smoller S, Wong ND, Wylie-Rosett J. Heart disease and stroke statistics—2010 update: a report from the American Heart Association. *Circulation*. 2010;121:e46–e215.
2. Chambers BR, Donnan GA. Carotid endarterectomy for asymptomatic carotid stenosis. *Cochrane Database Syst Rev*. 2005;4:CD001923.
3. Virmani R, Burke AP, Farb A, Kolodgie FD. Pathology of the vulnerable plaque. *J Am Coll Cardiol*. 2006;47:C13–18.
4. Virmani R, Ladich ER, Burke AP, Kolodgie FD. Histopathology of carotid atherosclerotic disease. *Neurosurgery*. 2006;59:S219–227; discussion S3–13.
5. Virmani R, Kolodgie FD, Burke AP, Farb A, Schwartz SM. Lessons from sudden coronary death: a comprehensive morphological classification scheme for atherosclerotic lesions. *Arterioscler Thromb Vasc Biol*. 2000; 20:1262–1275.
6. Takaya N, Yuan C, Chu B, Saam T, Underhill H, Cai J, Tran N, Polissar NL, Isaac C, Ferguson MS, Garden GA, Cramer SC, Maravilla KR, Hashimoto B, Hatsukami TS. Association between carotid plaque characteristics and subsequent ischemic cerebrovascular events: a prospective assessment with MRI—initial results. *Stroke*. 2006;37:818–823.

7. Singh N, Moody AR, Gladstone DJ, Leung G, Ravikumar R, Zhan J, Maggisano R. Moderate carotid artery stenosis: MR imaging-depicted intraplaque hemorrhage predicts risk of cerebrovascular ischemic events in asymptomatic men. *Radiology*. 2009;252:502–508.
8. Iemolo F, Martiniuk A, Steinman DA, Spence JD. Sex differences in carotid plaque and stenosis. *Stroke*. 2004;35:477–481.
9. Hellings WE, Pasterkamp G, Verhoeven BAN, De Kleijn DPV, De Vries JPM, Seldenrijk KA, van den Broek T, Moll FL. Gender-associated differences in plaque phenotype of patients undergoing carotid endarterectomy. *J Vasc Surg*. 2007;45:289–296; discussion 296–297.
10. Yuan C, Mitsumori LM, Ferguson MS, Polissar NL, Echelard D, Ortiz G, Small R, Davies JW, Kerwin WS, Hatsukami TS. In vivo accuracy of multispectral magnetic resonance imaging for identifying lipid-rich necrotic cores and intraplaque hemorrhage in advanced human carotid plaques. *Circulation*. 2001;104:2051–2056.
11. Hatsukami TS, Ross R, Polissar NL, Yuan C. Visualization of fibrous cap thickness and rupture in human atherosclerotic carotid plaque in vivo with high-resolution magnetic resonance imaging. *Circulation*. 2000;102:959–964.
12. Toussaint JF, LaMuraglia GM, Southern JF, Fuster V, Kantor HL. Magnetic resonance images lipid, fibrous, calcified, hemorrhagic, and thrombotic components of human atherosclerosis in vivo. *Circulation*. 1996;94:932–938.
13. Clarke SE, Hammond RR, Mitchell JR, Rutt BK. Quantitative assessment of carotid plaque composition using multicontrast MRI and registered histology. *Magn Reson Med*. 2003;50:1199–1208.
14. Trivedi RA, U-King-Im J, Graves MJ, Horsley J, Goddard M, Kirkpatrick PJ, Gillard JH. MRI-derived measurements of fibrous-cap and lipid-core thickness: the potential for identifying vulnerable carotid plaques in vivo. *Neuroradiology*. 2004;46:738–743.
15. Ota H, Yarnykh VL, Ferguson MS, Underhill HR, DeMarco JK, Zhu DC, Oikawa M, Dong L, Zhao X, Collar A, Hatsukami TS, Yuan C. Carotid intraplaque hemorrhage imaging at 3.0-Tesla MRI: a comparison of the diagnostic performance of three T1-weighted sequences. *Radiology*. 2009;254:551–563.
16. Cai J, Hatsukami TS, Ferguson MS, Kerwin WS, Saam T, Chu B, Takaya N, Polissar NL, Yuan C. In vivo quantitative measurement of intact fibrous cap and lipid-rich necrotic core size in atherosclerotic carotid plaque: comparison of high-resolution, contrast-enhanced magnetic resonance imaging and histology. *Circulation*. 2005;112:3437–3444.
17. Altaf N, MacSweeney ST, Gladman J, Auer DP. Carotid intraplaque hemorrhage predicts recurrent symptoms in patients with high-grade carotid stenosis. *Stroke*. 2007;38:1633–1635.
18. Zhu DC, Ferguson MS, DeMarco JK. An optimized 3D inversion recovery prepared fast spoiled gradient recalled sequence for carotid plaque hemorrhage imaging at 3.0 T. *Magn Reson Imaging*. 2008;26:1360–1366.
19. Underhill HR, Yarnykh VL, Hatsukami TS, Wang J, Balu N, Hayes CE, Oikawa M, Yu W, Xu D, Chu B, Wyman BT, Polissar NL, Yuan C. Carotid plaque morphology and composition: initial comparison between 1.5- and 3.0-T magnetic field strengths. *Radiology*. 2008;248:550–560.
20. DeMarco JK, Huston J, Nash AK. Extracranial carotid MR imaging at 3T. *Magn Reson Imaging Clin N Am*. 2006;14:109–121.
21. Beneficial effect of carotid endarterectomy in symptomatic patients with high-grade carotid stenosis. North American Symptomatic Carotid Endarterectomy Trial Collaborators. *N Engl J Med*. 1991;325:445–453.
22. Mullahy J. Much ado about two: reconsidering retransformation and the two-part model in health econometrics. *J Health Econ*. 1998;17:247–281.
23. Ammar AD, Mullins JR. Incidence of bilateral intraplaque hemorrhage in carotid artery disease. *Cardiovasc Surg*. 1993;1:717–719.
24. Saam T, Underhill HR, Chu B, Takaya N, Cai J, Polissar NL, Yuan C, Hatsukami TS. Prevalence of American Heart Association type VI carotid atherosclerotic lesions identified by magnetic resonance imaging for different levels of stenosis as measured by duplex ultrasound. *J Am Coll Cardiol*. 2008;51:1014–1021.
25. Endarterectomy for asymptomatic carotid artery stenosis. Executive Committee for the Asymptomatic Carotid Atherosclerosis Study. *JAMA*. 1995;273:1421–1428.
26. Prevention of disabling and fatal strokes by successful carotid endarterectomy in patients without recent neurological symptoms: randomised controlled trial. *Lancet*. 2004;363:1491–1502.
27. D'Agostino RB, Vasan RS, Pencina MJ, Wolf PA, Cobain M, Massaro JM, Kannel WB. General cardiovascular risk profile for use in primary care: the Framingham Heart Study. *Circulation*. 2008;117:743–753.

ORIGINAL RESEARCH

MR Carotid Plaque Imaging and Contrast-Enhanced MR Angiography Identifies Lesions Associated with Recent Ipsilateral Thromboembolic Symptoms: An In Vivo Study at 3T

J.K. DeMarco
H. Ota
H.R. Underhill
D.C. Zhu
M.J. Reeves
M.J. Potchen
A. Majid
A. Collar
J.A. Talsma
S. Potru
M. Oikawa
L. Dong
X. Zhao
V.L. Yarnykh
C. Yuan

BACKGROUND AND PURPOSE: Recent research has suggested the importance of plaque composition to identify patients at risk for stroke. This study aims to identify specific plaque features on 3T carotid MR imaging and CE-MRA associated with recent carotid thromboembolic symptoms in patients with mild/moderate versus severe stenosis.

MATERIALS AND METHODS: Ninety-seven consecutive patients (symptomatic, 13; asymptomatic, 84) with 50%–99% stenosis by sonography or CT angiography underwent carotid plaque imaging combined with MRA at 3T. The symptomatic carotid artery or the most stenotic asymptomatic carotid artery was chosen as the index vessel to be analyzed. Plaque features were compared by symptomatic status in patients with mild/moderate (30%–70%) versus severe (70%–99%) stenosis on MRA.

RESULTS: Ninety (92.8%) patients had sufficient image quality for interpretation. In 50 patients with mild/moderate stenosis, there were significant associations between the presence of the following plaque characteristics and symptoms: thin/ruptured fibrous cap (100% versus 36%, $P = .006$) and lipid-rich necrotic core (100% versus 39%, $P = .022$), with marginal association with hemorrhage (86% versus 33%, $P = .055$). In 40 patients with severe stenosis, only the angiographic presence of ulceration (86% versus 36%, $P = .039$) was associated with symptoms.

CONCLUSIONS: Several plaque components identified on 3T MR imaging are correlated with recent ipsilateral carotid thromboembolic symptoms. These preliminary results also suggest that associations between plaque characteristics and symptom history may vary by degree of stenosis. If confirmed in larger studies, carotid MR imaging may distinguish stable from unstable lesions, particularly in individuals with mild/moderate stenosis in whom the role of surgical intervention is currently unclear.

ABBREVIATIONS: AUC = area under the curve; CEA = carotid endarterectomy; CE-MRA = contrast-enhanced MRA; CE-T1WI = contrast-enhanced T1WI; CI = confidence interval; n/a = not applicable; MRA = MR angiography; NASCET = North American Symptomatic Carotid Endarterectomy Trial; OR = odds ratio; ROC = receiver operating characteristic analysis; T1WI = T1-weighted precontrast imaging; T2WI = T2-weighted imaging; TIA = transient ischemic attack; TOF = time-of-flight

Stroke is a leading cause of long-term disability and the third most common cause of mortality in the United States.[1,2] Large randomized trials such as the NASCET or the European Carotid Surgery Trial have shown the benefit of CEA for recently symptomatic patients with severe (≥70%) stenosis. The optimal treatment strategy in symptomatic patients with mild/moderate (30%–70%) carotid stenosis or in asymptomatic patients, however, remains unclear. For example, additional evaluation of the NASCET data found that of the 2226 symptomatic subjects with <70% stenosis, 61% had <50% stenosis.[3] The role of CEA in asymptomatic individuals is also still much debated in light of the results of the Asymptomatic Carotid Atherosclerosis Study[4] and the Asymptomatic Carotid Surgery Trial.[5] Various interpretations of these 2 studies have lead to discrepant recommendations of optimal treatment strategies.

To investigate the potential differences in carotid plaque characteristics, several studies have compared the histology of carotid plaques removed from symptomatic and asymptomatic patients who have undergone CEA. In a summation analysis of 7 such studies in which CEA specimens were removed from symptomatic and asymptomatic patients with equal severity of stenosis, Golledge et al[6] reported that histologic fea-

Received November 17, 2009; accepted after revision March 1, 2010.

From the Departments of Radiology (J.K.D., H.O., D.C.Z., M.J.P.), Epidemiology (M.J.R.), Neurology and Ophthalmology (A.M.); College of Human Medicine (J.A.T.); and College of Osteopathic Medicine (S.P.), Michigan State University, East Lansing, Michigan; Department of Radiology (H.R.U., M.O., L.D., X.Z., V.L.Y., C.Y.), University of Washington, Seattle, Washington; and Great Lakes Heart Lung and Vascular Institute (A.C.), Lansing, Michigan.

This work was supported by the American Heart Association Midwest Affiliate Grant-in-Aid 0855604G; Michigan State University/Office of Vice-President for Research & Graduate Studies and the Office of the Provost through the Internal Grant Program 05-IRGP-472; Bracco Diagnostic Inc; Extramural Research grant I021764; and National Institutes of Health grant HL56874.

Paper previously presented in part at: 17th Scientific Meeting of the International Society for Magnetic Resonance in Medicine, April 18–24, 2009; Honolulu, Hawaii.

Please address correspondence to J. Kevin DeMarco, MD, Department of Radiology, Michigan State University, 184 Radiology Bldg, East Lansing, MI 48824; e-mail: jkd@rad.msu.edu

DOI 10.3174/ajnr.A2213

tures of surface ulceration and plaque rupture along with fibrous cap thinning were associated with ipsilateral carotid symptoms in all the studies. However, the association between histologically identified plaque hemorrhage and lipid-rich necrotic core with symptoms was less clear in the study by Golledge et al. Intraplaque hemorrhage was equally common in symptomatic and asymptomatic patients (48% versus 50%) with severe stenosis requiring CEA, and no significant differences in the presence or size of the lipid-rich necrotic core between symptomatic and asymptomatic patients were noted in 6 of the 7 studies.

In a more recent and larger systematic review of 31 observational studies, Gao et al[7] again noted the lack of correlation of intraplaque hemorrhage with symptoms in large, recent, or high-quality studies. While these reviews of CEA histology confirm that some plaque features are associated with symptoms, there is a clear gap in the histology-based literature in patients with <70% stenosis who do not undergo surgery. Thus, the importance of plaque characteristics and symptom history in patients with mild/moderate stenosis is unknown. MR imaging of carotid plaque in patients with mild/moderate and severe stenosis could help fill this gap in the histologic literature.

The advent of vessel wall imaging for the in vivo evaluation of atherosclerotic disease, particularly carotid atherosclerotic disease, has shifted the focus toward the preoperative evaluation of plaque composition that may identify unstable lesions.[8-13] Direct in vivo 3T MR imaging of carotid plaque may be useful in identifying patients with an increased risk of ipsilateral thromboembolic symptoms. Carotid plaque MR imaging may be particularly helpful in symptomatic or asymptomatic patients with <70% carotid stenosis for whom there is a lack of histologic studies of carotid plaque as well as a lack of consensus agreement on the optimal treatment strategy.

CE-MRA can demonstrate the degree of carotid stenosis compared with digital subtraction angiography, especially when care is taken to maintain submillimeter in-plane resolution.[14,15] Recent work has demonstrated that ultra-high-resolution carotid CE-MRA on the order of 0.28 mm^3 is possible with dedicated carotid surface coils on a 3T MR imaging scanner.[16] Ultra-high-resolution carotid CE-MRA may depict luminal changes related to underlying plaque pathology that are associated with symptoms.

The purpose of this study was to identify atherosclerotic plaque features on high-spatial-resolution carotid 3T MR imaging and CE-MRA associated with recent ipsilateral carotid thromboembolic symptoms that may represent unstable plaque in patients with mild/moderate (30%–69%) carotid stenosis. In addition, we wanted to test the hypothesis that plaque features associated with symptoms may differ between patients with mild/moderate versus severe (70%–99%) carotid stenosis.

Materials and Methods

Our study was compliant with the Health Insurance Portability and Accountability Act and was approved by the local institutional review board. Consent forms signed by patients at the time of imaging allowed retrospective analysis of patient studies and data. Bracco Diagnostic, which provided some grant support for this project, had no input into the formulation of this article.

Subjects

Between August 2005 and March 2007, 97 consecutive patients, under the care of the referring vascular surgeon or stroke neurologist, with carotid artery stenosis of 50%–99% involving 1 or both carotid bifurcations identified with noninvasive imaging such as duplex sonography or CT angiography, underwent carotid MR imaging. Of the 97 patients, 13 were neurologically symptomatic with a history of TIA, amaurosis fugax, or stroke appropriate to the distribution of the carotid artery within the past 4 months as confirmed by the referring vascular surgeon with >20 years of clinical experience or the referring stroke neurologist with >10 years of clinical experience. Other possible etiologies of thromboembolic disease were excluded from the study. These cases were identified by the referring vascular surgeon and stroke neurologists following work-up with an electrocardiogram and transthoracic echocardiography. If a patent foramen ovale was detected, additional lower extremity duplex sonography to exclude deep venous thrombosis was performed. Additional telemetry and transesophageal echocardiography were performed in patients in whom there was a high clinical suspicion of thromboembolic cardiac disease. Patients with other possible etiologies of thromboembolic disease who were identified by the vascular surgeon or stroke neurologist were excluded before imaging. The remaining 84 patients were asymptomatic. Clinical information was obtained through patient interview and supplemented with a chart review.

MR Imaging Protocol

Patients were imaged with a 3T whole-body MR imaging scanner and a research 4-channel phased-array surface coil.[17] The artery selected for imaging, termed the "index artery," was determined by symptom status. The symptomatic carotid artery with 50%–99% stenosis or the most stenotic asymptomatic carotid artery as previously determined by duplex sonography or CT angiography was chosen as the index vessel to be analyzed. MR images with 4 different types of contrast were obtained, including 3D TOF images, quadruple inversion recovery precontrast T1WI, multisection double inversion T2WI, and quadruple inversion recovery CE-T1WI obtained 5 minutes after intravenous infusion of 0.15-mmol gadobenate dimegulamine per kilogram of body weight.

These protocols were performed in a manner similar to the previously published standardized protocol for a 1.5T scanner,[18] except that a longer TR on the T2WI sequence was used to avoid unwanted T1 weighting at 3T.[19] The in vivo 3T MR imaging protocol details are presented in Table 1. The black-blood T2WI was obtained with a time-efficient multisection double inversion recovery blood-suppressed technique[20] with TIs adjusted for blood T1 at 3T. Pre- and postcontrast black-blood T1WI was acquired by using a quadruple inversion recovery sequence that provided T1-insensitive blood suppression.[21] The postcontrast black-blood T1WI was obtained 5 minutes after injection of contrast. Fat suppression was used for T1WI and T2WI to reduce the signal intensity from subcutaneous fat. All images were acquired in the transverse plane and were centered to include both carotid bifurcations and the regions of carotid stenosis identified on rapid-screening 2D TOF MRA, which evaluated the middle 15 cm of the neck. In cases in which the carotid bifurcation or regions of carotid stenosis were at disparate levels in the neck as seen on the screening 2D TOF MRA, additional coverage in the superior-inferior direction was obtained as needed by adding extra transverse images for the dedicated carotid plaque series. After bolus gadolinium contrast intravenous injection, a very high-resolution (0.28 mm^3)

Table 1: Parameters for carotid MR imaging protocols at 3T

Parameter	T1WI With or Without Contrast Enhancement	T2WI	TOF Imaging	CE-MRA
Acquisition mode	2D	2D	3D	3D
Acquisition sequence	Fast spin-echo	Fast spin-echo	Spoiled gradient and flow compensation	Enhanced gradient recalled-echo
Blood suppression technique	Quadruple inversion recovery	Multisection double inversion recovery	Saturation veins	None
TE (ms)	11	52	3.5	1.7
TR (ms)	800	4000	23	5.5
TI (ms)	520	250	n/a	n/a
Echo-train length	10	12	n/a	n/a
Excitation flip angle (degrees)	90	90	20	30
No. of signals acquired	1	2	1	
FOV[a]	160 × 130 mm	160 × 120 mm	160 × 160 mm	150 mm
Matrix size	256 × 256	256 × 256	288 × 256	256 × 256
No. of sections	18	18	48	40
Section thickness (mm)	2	2	1	0.8
Coverage (mm)	36	36	44	32 mm
Imaging time (min:sec)	5:49	4:32	4:46	0:59

[a] The FOV of 140 × 140 cm was also used in some patients.

coronal elliptical-centric carotid MRA was performed with a test bolus to time the contrast arrival.[16]

A pair of experienced reviewers who were blinded to clinical information performed image review by using a previously described protocol.[19] In brief, a pair of reviewers taken from a total pool of 7 reviewers, all with >1.5 years of experience in carotid plaque imaging and blinded to subject, time point, and site information, reviewed the MR images. Differing pairs of reviewers were chosen to evaluate each of the research carotid plaque studies. Each scan was read by these 2 reviewers to reach a consensus decision. An image-quality rating (4-point scale: 1 = poor, 4 = excellent) was assigned to all MR images before the review. For images with image-quality scores of ≥2, image-analysis software (CASCADE[18,22]) was used to draw the lumen and outer wall boundaries. The arterial wall area was recorded along with various plaque features, including lipid-rich necrotic core, calcification, and hemorrhage, determined according to previously published criteria that have been validated with histology[18,22] based on relative tissue signal intensities on TOF, T1WI, T2WI, and CE-T1WI compared with the adjacent sternocleidomastoid muscle. Details of the criteria are as follows: Lipid-rich necrotic core without hemorrhage is isointense on TOF images and T1WI, hypointense on CE-T1WI, and hypointense on T2WI; calcification shows hypointensity on all the image weightings; and hemorrhage appears hyperintense on TOF images and T1WI and can be hypointense to hyperintense on T2WI.

In sections with a lipid-rich necrotic core, fibrous cap status (intact thick, intact thin, or disrupted cap) was evaluated on the basis of previously published criteria.[22,23] Intact thick fibrous caps showed a uniform dark band adjacent to the lumen on TOF, an enhanced band adjacent to the lumen on CE-T1WI, and a smooth luminal surface on all the images. Intact thin caps showed no visible dark band adjacent to the lumen on TOF, no visible enhanced band adjacent to the lumen on CE-T1WI, and a smooth luminal surface on all the images. Ruptured fibrous cap showed a disrupted dark band or no visible dark band adjacent to the lumen on TOF, an irregular luminal surface on all the images, and a hyperintense area adjacent to the lumen on TOF images.

An image-analysis software package[24] was used to record measurements of the lumen area, wall area, wall thickness, and the area of tissue components when present.[10,18,25] For plaque composition, the proportion of wall volume occupied by that feature was calculated for each artery (percentage volume). This calculation normalizes compositional features to the vessel size to account for innate differences in arterial size between subjects.

Last, 2 experienced reviewers who were blinded to clinical outcome and carotid plaque findings reviewed all MRAs. A consensus decision was reached for the presence or absence of an ulcerated lumen based on previously published standards.[26] The measurement of percentage diameter carotid stenosis was based on the NASCET criteria from the high-resolution carotid CE-MRA on multiplanar reformations generated by using a 3D stand-alone workstation.[27] For this study, severe stenosis was defined, by using NASCET criteria, as a percentage diameter stenosis between 70% and 99% on CE-MRA. When the percentage diameter stenosis measured 30%–69% on the CE-MRA, the patient was categorized as having a mild-to-moderate stenosis.

Statistical Analysis

Each patient contributed only 1 set of observations (ie, the index carotid artery) to the dataset for analysis. All the categoric and continuous features were analyzed on an artery/patient basis. For each continuous metric of MR imaging–identified plaque components, the percentage volume from each artery was analyzed. The minimal lumen area and the maximal wall thickness were also used during data analysis. Descriptive statistics are presented as mean ± SD for continuous variables and as numbers of cases and percentages for categoric variables. Prevalence and size of plaque features were compared between patients with mild/moderate and severe carotid stenosis by using either a χ^2 test for categoric variables or a Student t test for continuous variables.

The magnitude of the association between carotid artery characteristics as identified by MR imaging and recent cerebrovascular symptoms was determined separately for the mild/moderate and severe stenosis groups by using univariate logistic regression. Results from logistic regression analysis are reported as an OR with a 95% CI. We used exact logistic methods to calculate the lower limit of the 95% CI for the OR as well as the Fisher exact test to determine the statistical significance of the associations between recent symptoms and the presence or absence of plaque characteristics in the presence of zero